

Elemental abundances of high redshift quasars [★]

M. Dietrich^{1,2} and U. Wilhelm-Erkens¹

¹ Landessternwarte Heidelberg, Königstuhl, 69117 Heidelberg, Germany

² Department of Astronomy, University of Florida, 211 Bryant Space Science Center, Gainesville, FL 32611-2055, USA

Received 12 August 1999 / Accepted 13 December 1999

Abstract. A sample of 16 high redshift quasars with $2.4 \lesssim z \lesssim 3.8$ was observed with moderate spectral resolution in the restframe ultraviolet. The emission-line fluxes of NV 1240, CIV 1549, and HeII 640 were used to estimate the metallicity of the line emitting gas. The line ratios were investigated within the frame work of models presented by Hamann & Ferland (1992, 1993, 1999). The scaled solar abundance model yields inconsistent results for the metallicity while the rapid star formation scenario is successful in indicating a common range of overabundance on base of NV1240/CIV1549 and NV1240/HeII1640 line ratios. We estimated an abundance of $Z \simeq 8 Z_{\odot}$ of the line emitting gas given by NV/CIV and NV/HeII. Assuming an evolution time scale of ~ 1 Gyr and a cosmological model with $\Omega_M \simeq 0.3$, $\Omega_{\Lambda} \simeq 0.7$, and $H_0 \simeq 65 \text{ km s}^{-1} \text{ Mpc}^{-1}$ the first violent star formation epoch should start at a redshift of $z_f \simeq 6$ to 10.

Key words: galaxies: quasars: emission lines – galaxies: quasars: general – cosmology: early Universe

1. Introduction

Quasars are among the most luminous objects known in the universe. Due to their high luminosity they can be observed easily to redshifts of $z \simeq 5$ or even more. Currently, nearly 100 quasars with redshifts larger than $z = 4$ are known and recently the first quasar with $z = 5.0$ was discovered by Fan et al. (1999) in late 1998. The redshift range of $z \geq 3$ corresponds to an epoch when the universe had an age of approximately 10 % of its current age (assuming $H_0 = 65 \text{ km s}^{-1} \text{ Mpc}^{-1}$, $\Omega_M = 0.3$, $\Omega_{\Lambda} = 0.7$; cf. Carroll et al. 1992; Carlberg et al. 1999; Perlmutter et al. 1999). Therefore, quasars provide a powerful probe to study the early history of the universe. Especially, with respect to dating the first star

formation epoch quasars have gained increasing interest. Their prominent emission-line spectrum can be used a diagnostic tool to estimate the enrichment of the gas with heavy elements due to violent star formation (for a review see Hamann & Ferland 1999).

Recent studies of quasars at high redshift ($z \geq 3$) provide evidence for significantly enhanced metallicities up to an order of magnitude compared to solar metallicities (cf. Hamann & Ferland 1992, 1993; Ferland et al. 1996; Korista et al. 1996; Pettini 1999). These derived high metallicities require a violent star formation phase.

The prominent spectra of quasars provide much information on the physical conditions and the elemental abundances of the gas. But the emission line strength is quite insensitive to metallicity effects. For example, the $\text{Ly}\alpha/\text{CIV}1549$ ratio is nearly independent to heavy element abundances (Hamann & Ferland 1999). However, there are several emission line ratios which are sensitive to relative abundance ratios and these can be used to put constraints on both the metallicity and evolution parameters.

The key of the approach using those line ratios to estimate the metallicity are the different time scales of the enrichment of gas with α -elements like oxygen, neon, or magnesium, carbon as an additional primary element, nitrogen as a secondary element, or iron. While α -elements are produced predominantly in massive stars on short time scales the production of C as a primary and N as a secondary element is ascribed to intermediate mass stars which evolve on significant longer time scales. The dominant source of iron is given by SN Ia explosions which are ascribed stars of intermediate mass (cf. Wheeler et al. 1989).

Previous investigations to estimate the abundances in BELR gas based on the measurement of several generally weak inter-combination lines like NIV]1486, OIII]1663, NIII]1750, and CIII]1909 (cf. Shields 1976; Davidson 1977; Baldwin & Netzer 1978; Osmer 1980; Gaskell et al. 1981; Uomoto 1984). Furthermore, and even more serious these lines are subject to collisional de-excitation for densities larger than $n_e = 10^{10} \text{ cm}^{-3}$. In spite of these limitations and of the current assumption of higher densities of the BLR gas (Rees et al. 1989; Ferland et al. 1992; Peterson 1993; Baldwin et al. 1995) the results of the early estimates indicate larger than solar metallicities for the BELR gas. Since the investigations of Hamann & Ferland (1992, 1993), Osmer et

Send offprint requests to: M. Dietrich

[★] Based on observations collected at the German-Spanish Astronomical Centre, Calar Alto, operated by the Max-Planck-Institut für Astronomie (MPIA), Heidelberg, jointly with the Spanish National Commission for Astronomy; McDonald Observatory/Texas, University of Austin/TX, USA; the VLT-UT1 operated on Cerro Paranal (Chile) by the European Southern Observatory, *Present address:* Department of Astronomy, University of Florida

Correspondence to: e-mail: dietrich@astro.ufl.edu

al. (1994), and Ferland et al. (1996) alternative line ratios gain increasing interest. The NV1240 emission is of special interest since this emission line of a secondary element is generally stronger than expected in the spectra of high redshift quasars in the frame work of standard photoionization models. Hamann & Ferland (1992, 1993) showed that NV1240/CIV1549 and NV1240/HeIII1640 can be used as robust metallicity indicators. However, NV1240 and HeIII1640 are generally difficult to measure since both lines are severely blended by Ly α and CIV1549, OIII]1663, respectively.

In Sect. 2 we described the observations and the data analysis of our sample of 16 quasars with redshift $z \approx 3$. In Sect. 3 we present the results of the analysis of the emission line spectra. We derived the elemental abundance of the line emitting gas based on the line ratios of several diagnostic emission lines. While the line ratio Ly α /CIV1549 is nearly independent of metallicity effects NV1240/CIV1549 and NV1240/HeIII1640 provide suitable information to estimate the elemental abundance of the line emitting gas (e.g. Ferland et al. 1996; Korista et al. 1997; Hamann & Ferland 1999). Using these emission-line ratios we derived elemental abundances of $Z \sim 8 Z_{\odot}$ for the BELR gas of the quasar sample we observed. The results are discussed and are compared with recent studies (e.g. Ferland et al. 1996; Hamann & Ferland 1999). Our results provide further evidence that the first violent star formation epoch might start at a redshift of $z_f \approx 6$ to 10.

2. Observations and data analysis

We used most of the published QSO surveys (Condon et al. 1977; Foltz et al. 1989; MacAlpine et al. 1977; MacAlpine & Feldman 1982; Olsen 1970; Sargent et al. 1989; Schneider et al. 1991, 1992; Schmidt et al. 1987; Steidel et al. 1991; Wolfe et al. 1986) and also parts of the Hamburg QSO survey (Reimers et al. 1989; Hagen 1993) to compile an appropriate sample of high redshift quasars. The redshift range of $2.7 \lesssim z \lesssim 3.3$ was chosen to assure that most of the diagnostic ultraviolet emission lines are shifted to the optical regime. Generally, the spectra of high redshift quasars are contaminated by absorption line systems like damped Ly α systems and the Ly α -forest. We selected quasars with no strong contamination since we are predominantly interested in the emission line flux and profiles. The quasars had to be brighter than 20 mag to achieve a sufficient S/N ratio of at least 20 for the continuum for reasonable integration times for observations with telescopes of the 3 m class. This original sample was complemented by four quasars which were observed with the VLT UT 1 Antu.

We observed the 16 quasars of our sample at Calar Alto Observatory/Spain (August 1993), McDonald Observatory/USA (July 1995), and at Paranal/Chile (Sept., Oct., and December 1998). In Table 1 the quasars and details to the observations are listed. The name of the quasar is given in (1), the coordinates α and δ denote column (2) and (3). In (4) the redshift of the quasars is listed. We measured the emission lines of Ly α , SiIV1400, and CIV1549 to determine the redshift. A Gaussian profile was fitted to the upper part of the line profile characterized by more

than 50 % of the peak intensity. The uncertainty of the measured redshift is of the order of $\text{rms}(z) = 0.01$. The apparent and absolute magnitude are given in (5) and (6), respectively. The date of the observation is given in column (7) and the integration time in (8). Finally, the site of the observations is listed in column (9).

At Calar Alto Observatory we used the twin-spectrograph which was attached to the Cassegrain focus of the 3.5 m telescope. Tektronix CCD detectors with 1024×1024 pixels were mounted in both channels. Gratings with 72 \AA/mm and 108 \AA/mm were used in the blue and red channel of the twin-spectrograph, respectively. In the blue channel a wavelength range of $3700 - 5505 \text{ \AA}$ was covered while the red channel provided a coverage from $5465 - 8180 \text{ \AA}$. The overlap of the spectra of the blue and red channel amounts to at least 20 \AA around $\lambda = 5500 \text{ \AA}$. The slit width was fixed to $1''.76$ projected on the sky for both channels and a fixed position angle of $\text{PA} = 0^\circ$. For all exposures the hour angle of the quasars was less than 30° to minimize the light loss caused by differential refraction. Furthermore, the effect was less than $0''.4$ for the zenithal distance of the objects during the exposures.

Helium-argon spectra were taken after each object exposure for wavelength calibration. The relative uncertainty of the calibration amounts to $\Delta\lambda = \pm 0.2 \text{ \AA}$. Spectra of the standard stars BD+26 $^\circ$ 2606, BD+33 $^\circ$ 2642, BD+28 $^\circ$ 4211, and Feige110 were observed for flux calibration each night (Massey et al. 1988; Oke 1990; Oke & Gunn 1983; Turnshek 1990). The quasars and the standard stars observed for flux calibration can be taken as point sources. Therefore, the light loss due to the slit width used is nearly identical especially because the seeing during the observations was quite constant at $1''.5 \pm 0''.5$. Furthermore, our main interest is relative line flux ratios and the corresponding emission line profiles hence we recorded the spectra with a slit width of $1''.76$ only to obtain a spectral resolution which is sufficient to study the line ratio for different parts of the line profile.

The observations at the McDonald Observatory/USA were obtained with the 2.7 m telescope using the LCS longslit spectrograph. The measurements were recorded with the CC1 CCD with 1024×1024 pixel elements, pixel size $12 \mu\text{m}^2$. The position angle of the slit was set to $\text{PA} = 0^\circ$ and a fix slit width of $2''$ was selected. The hour angle of the quasars was less than $\sim 30^\circ$ to ensure that the light loss due to differential refraction is minimized. To obtain a continuous spectral coverage of $3780 - 7820 \text{ \AA}$ we used three settings with grating #43 ($3780 - 5200 \text{ \AA}$) and #44 ($5100 - 6500 \text{ \AA}$, $6400 - 7820 \text{ \AA}$). Hence, the overlap of the orders amounts to $\approx 100 \text{ \AA}$. Argon neon spectra were taken after each object exposure for wavelength calibration. Spectra of the standard stars BD+33 $^\circ$ 2642 and BD+28 $^\circ$ 4211 were observed for flux calibration each night.

In addition we used FORS 1 attached at the VLT UT 1 Antu during the commissioning and scientific observations in September, October, and December 1998 to observe four quasars with redshifts larger than $z = 3.0$ (Dietrich et al. 1999). Since the objective of these observations was to check and derive instrumental functions and parameters, very different observational conditions and relatively short exposure times were used.

Table 1. Observation log of the high redshift quasars

Object	R.A. (2000.0)	Decl. (2000.0)	z_{em}^a	m_V^b	M	date	t_{int} [sec]	site ^c
(1)	(2)	(3)	(4)	(5)	(6)	(7)	(8)	(9)
UM196	00 01 50	-01 59 41	2.81	18.0	-28.7	Aug. 14 1993	1800	CA
						Aug. 14 1993	3600	CA
						Aug. 17 1993	2400	CA
Q0044-273	00 47 11	-27 04 41	3.16	20.3	-27.5	Oct. 04 1998	900	Para
						Oct. 04 1998	1800	Para
UM667	00 47 50	-03 25 11	3.13	18.6	-28.7	Aug. 15 1993	3600	CA
						Aug. 17 1993	3600	CA
Q0046-282	00 49 24	-27 59 02	3.83	19.7	-28.7	Sep. 22 1998	600	Para
						Sep. 22 1998	600	Para
Q0103-294	01 06 03	-29 08 59	3.12	20.2	-27.7	Sep. 25 1998	900	Para
						Sep. 25 1998	900	Para
						Sep. 25 1998	1200	Para
Q0103-260	01 06 04	-25 46 53	3.36	18.8	-28.9	Sep. 24 1998	900	Para
						Sep. 24 1998	900	Para
						Sep. 24 1998	1800	Para
						Dec. 16 1998	1800	Para
						Dec. 19 1998	1800	Para
						Dec. 26 1998	1800	Para
4C25.05	01 26 43	+25 59 02	2.36	17.5	-29.1	Aug. 13 1993	2700	CA
Q0216+0803	02 18 57	+08 17 28	2.99	18.1	-29.4	Jul. 29 1995	3600	McD
						Jul. 30 1995	5002	McD
						Jul. 31 1995	4640	McD
HS1425+60	14 25 33	+60 39 16	3.19	16.9	-30.3	Aug. 13 1993	3600	CA
						Aug. 16 1993	3600	CA
Q1548+0917	15 51 03	+09 08 50	2.75	18.0	-29.2	Jul. 29 1995	4500	McD
						Jul. 30 1995	4500	McD
						Jul. 31 1995	4800	McD
						Aug. 01 1995	760	McD
						Aug. 01 1995	3001	McD
PC1640+4711	16 41 26	+47 05 46	2.77	19.5	-27.7	Jul. 29 1995	1800	McD
						Jul. 30 1995	5400	McD
						Jul. 31 1995	5400	McD
HS1700+64	17 00 41	+64 16 24	2.74	16.9	-30.4	Aug. 12 1993	3600	CA
						Aug. 14 1993	3600	CA
						Aug. 15 1993	3600	CA
Pks2126-15	21 29 12	-15 38 42	3.28	17.3	-30.0	Aug. 14 1993	1800	CA
						Aug. 15 1993	3600	CA
						Aug. 16 1993	3600	CA
PC2132+0126	21 35 11	+01 39 31	3.19	19.4	-27.6	Aug. 12 1993	1800	CA
						Aug. 12 1993	3600	CA
Q2231-0015	22 34 09	+00 00 01	3.02	17.5	-30.0	Aug. 13 1993	3600	CA
						Aug. 17 1993	3180	CA
						Jul. 29 1995	3600	McD
						Jul. 30 1995	5400	McD
						Jul. 31 1995	4800	McD
						Aug. 01 1995	1039	McD
UM659	23 14 06	-03 25 35	3.04	19.9	-27.6	Aug. 13 1993	1800	CA
						Aug. 13 1993	3600	CA
						Aug. 14 1993	3600	CA

^a measured from the Ly α , SiIV1400, CIV1549 emission lines^b taken from Hewitt & Burbidge 1993^c CA, 3.5 m telescope Calar Alto Observatory/Spain; McD, 2.7 m telescope McDonald Observatory/USA; Para, 8.2 m telescope VLT UT1 Antu Paranal/Chile

Two spectral wavelength ranges with different spectral resolutions were observed. With grism 150 I a wavelength range of $\sim 3300 - 11800 \text{ \AA}$ was covered and grism 600 B provided a spectral coverage of $\sim 3600 - 6000 \text{ \AA}$. The position angle of the slit was selected with respect to minimize the influence of the differential refraction. The slit width was set to $0''.7$ (Q0046-282, Q0103-294) and $1''.0$ (Q0044-273, Q0103-260). To obtain the highest possible spectral resolution Q0103-260 were observed also with grism 600B and a slit width of $0''.4$. For wavelength calibration helium-mercury-cadmium spectra were taken. For flux calibrations the standard star LTT 9491 was observed with the same grisms.

The 2D longslit spectra were reduced and analysed using standard MIDAS software. First, the spectra were bias subtracted and flatfield corrected. Cosmic-ray events on the CCD images were removed manually by comparing the individual spectra taken for each object. The night sky component of the 2D-spectra was subtracted by fitting Legendre polynomials of third order perpendicular to the dispersion. These polynomials were fitted on each spatial row of the spectra using areas on both sides of the object spectrum which were not contaminated by the quasar or other objects.

The 1D-spectra were derived using the Horne algorithm for optimal extraction (Horne 1986). The limits of the spatial extraction windows were chosen to 4σ as derived from the seeing during the observation. σ was derived from a Gaussian fit which was applied to the spatial profile of the spectrum. The wavelength calibration frames were used to rebin the extracted spectra obtained at Calar Alto to linear wavelength steps of 1.76 \AA and 2.64 \AA for the blue and the red channel, respectively. To check the absolute error of the wavelength calibration night sky spectra were extracted from the two-dimensional object frames and wavelength calibrated in the same way as the object spectra. The night sky lines (HgI 4047 \AA , HgI 4358 \AA , [OI] 6300 \AA , [OI] 6364 \AA) give an absolute uncertainty of $\text{rms}_\lambda \simeq 0.2 \text{ \AA}$ in the blue channel and $\text{rms}_\lambda \simeq 0.4 \text{ \AA}$ in the red channel. The spectral resolution was determined by measuring the FWHM of these night sky lines, too. The spectral resolution of the spectra taken at Calar Alto Observatory amounts to $\Delta\lambda = 4.0 \text{ \AA}$ and $\Delta\lambda = 5.2 \text{ \AA}$ in the blue and the red channel, respectively ($\Delta v \simeq 300 \text{ km s}^{-1}$). The achieved spectral resolution of the spectra obtained at McDonald Observatory was determined for the entire observed spectral range to be $\Delta\lambda \simeq 5.4 \text{ \AA}$. The quasars observed with FORS 1 were recorded with two different spectral resolutions which were determined from the FWHM of several strong night sky emission lines. With grism 150 I a spectral resolution of $\Delta\lambda \simeq 25 \text{ \AA}$ is achieved for a wavelength range of $\sim 3500 - 10000 \text{ \AA}$ and grism 600 B provide a spectral resolution of $\Delta\lambda \simeq 5.4 \text{ \AA}$ for a slit width of $1''$. The spectrum of Q 0103-260 taken with grism 600 B and a slit width of $0''.4$ yields a spectral resolution of $\Delta\lambda \simeq 2.9 \text{ \AA}$. The uncertainty of the wavelength calibration amounts to $\text{rms}_\lambda \simeq 0.35 \text{ \AA}$ for grism 150 I and $\text{rms}_\lambda \simeq 0.09 \text{ \AA}$ for grism 600 B, respectively.

We corrected each quasar spectrum for the atmospheric B-band at 6850 to 6900 \AA , the A-band at 7590 to 7690 \AA absorption which both are caused by O_2 , and the atmospheric a-band

7170 to 7400 \AA which is due to water vapor. The absorption features were linearly interpolated in the spectrum of the standard stars which were observed under comparable conditions. The ratio of the interpolated and the original spectrum gives the scaling factors for the correction of the atmospheric absorptions. However, for the four quasars recorded with FORS 1 no removal of the atmospheric absorption features was attempted. Therefore, the strong atmospheric A and B bands (at 7600 \AA and 6900 \AA) and are clearly visible in Fig. 1. On the other hand, as shown by Fig. 1, although affecting in some cases the outer wings of the broad emission lines, the atmospheric features had little effect on the line flux measurements.

For the correction of the atmospheric extinction we used the standard extinction curve of La Silla (Schwarz & Melnick 1993). The corresponding airmass was computed for the middle of each exposure. The interstellar extinction was corrected using the values of Burstein & Heiles (1982) and the extinction curve of Savage & Mathis (1979). Since the galactic latitude of the quasars observed with FORS 1 is less than $b = -86^\circ$ no correction for interstellar extinction were applied to these spectra.

The spectra observed at Calar Alto Observatory and McDonald Observatory were corrected for losses due to the differential refraction (Filippenko 1982). This was done using the MIDAS application refraction/long which was designed for point sources. For one quasar, Q2231-0015, we obtained spectra at Calar Alto Observatory and McDonald Observatory as well. The spectra were identical within less than 6% with respect to the overall continuum shape and emission-line strength.

The final step of the data reduction was the unweighted summation of the spectra for each quasar. Hence, the spectra of the three settings (McDonald Observatory) and two settings (Calar Alto Observatory) were rebinned to a uniform wavelength scale of 1 \AA .

3. Analysis and results

The flux calibrated spectra of the observed quasars are shown in Fig. 1 and 2. The flux is given in units of $10^{-15} \text{ erg s}^{-1} \text{ cm}^{-2} \text{ \AA}^{-1}$. The strongest lines in the spectra are Ly α , CIV1549, and CIII]1909. The broad $\lambda 1400 \text{ \AA}$ feature which consists of the SiIV1397,1403 and the OIV]1402 multiplet will be referred as SiIV1402 in the following. The strength of the SiIV1402 emission line displays a wide range relative to CIV1549. While HS 1700+64 and UM 667 show strong SiIV1402 emission it is much weaker in 4C25.05 and Q2231-0015 while it is nearly missing in Q 0044-273 (Figs. 1,2).

In addition to these emission lines several important diagnostic lines are visible like OVI1034, OII1304, CII1335, HeII1640, and OIII]1663. The intercombination line of NIII]1750 can be detected in UM196, Q1548+0917, HS1700+64, and Q2231-0015. For Q0103-294 an upper limit of the line strength of NIII]1750 can be estimated at least.

Before we measured the integrated emission line flux we had to correct the line profiles for absorption line contamination. Although, one of the selection criteria of the quasar sample was a minor influence of absorption line systems it cannot be totally

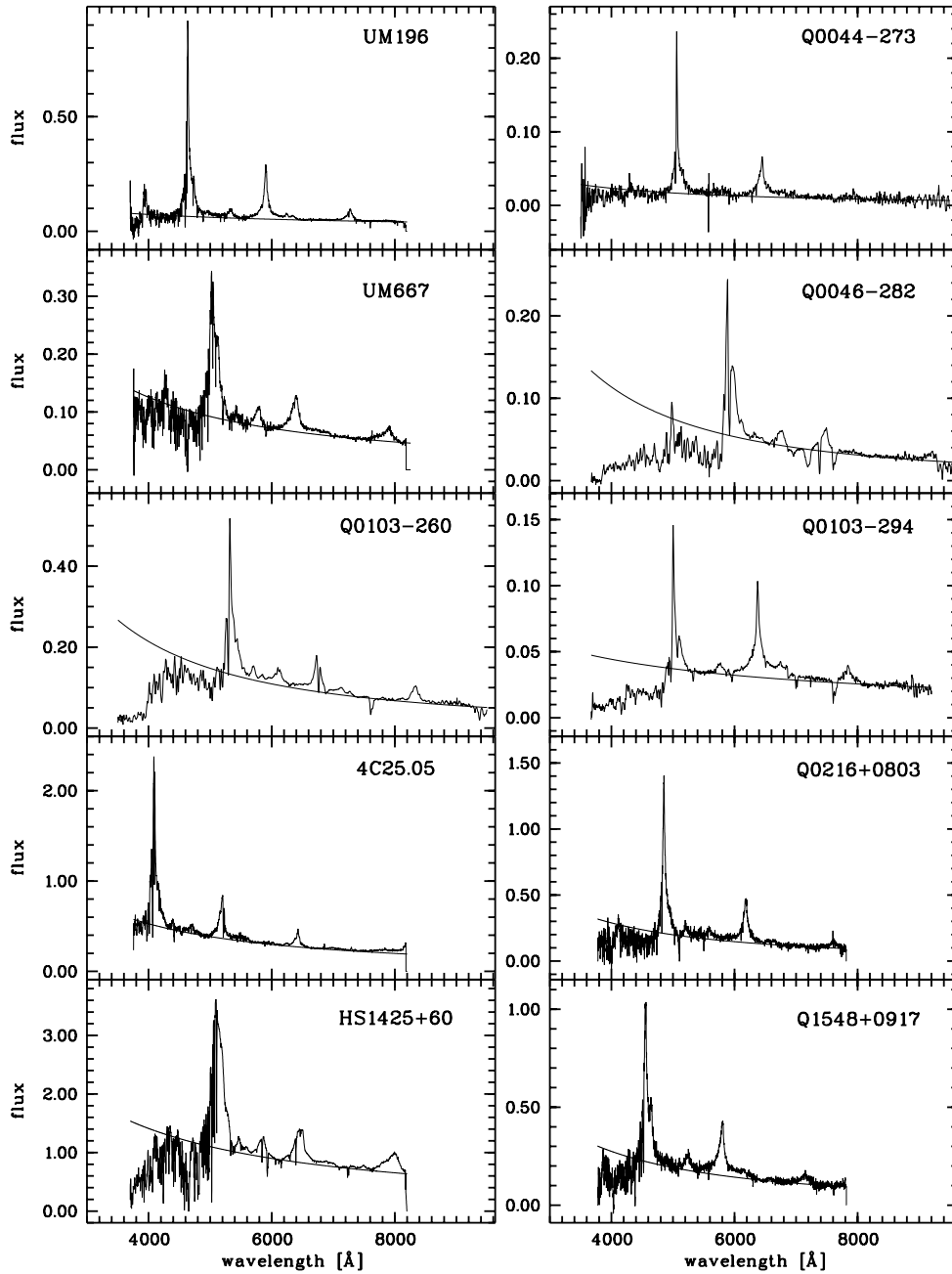


Fig. 1. The spectra of the observed quasars. The flux is given in units of $10^{-15} \text{ erg s}^{-1} \text{ cm}^{-2} \text{ \AA}^{-1}$. For each quasar the corresponding power law fit $F_\nu \sim \nu^{-\alpha}$ of a nonstellar continuum is displayed.

avoided for quasars at the observed high redshift of $z \simeq 3$. In the short wavelength regime, $\lambda_{\text{rest}} \leq 1215 \text{ \AA}$, Ly α absorption systems are visible while on the red side of Ly α some metal absorption line systems can be seen (Figs. 1, 2). We restored the contaminated emission line profiles by linear interpolation between adjacent peaks of the observed profile. To illustrate the method the result of this approach is shown in Fig. 3 for the Ly α profile of UM 196 and HS 1700+64. We performed the correction several times independently to the individual spectra to minimize the uncertainties introduced by the interpolation method described above. The corrected individual spectra of the distinct objects were averaged. The method to recover the line profiles by linear interpolation is sensitive to the spectral reso-

lution. Therefore, we rebinned the spectra which we obtained at Calar Alto Observatory/Spain and McDonald Observatory/USA to a lower spectral resolution and compared those with our corrected profiles. The peakness of the rebinned profile core was degraded as expected while the difference in the wings is of the order of less than 5%.

For the quasars observed with the VLT UT 1 Antu we obtained spectra of low and high spectral resolution for the Ly α range. The Ly α profile was corrected for absorption features independently. The corrected profiles of the different spectral resolution are in good agreement.

We used the corrected emission-line profiles to measure the line flux. Because the NV1240 and HeIII1640 profiles are

Table 2. Broad emission-line flux measurements for the observed quasar sample. In addition the spectral index α of the power law continuum fit $F_\nu \propto \nu^{-\alpha}$ is given.

	$F_{obs} [10^{-15} \text{ erg s}^{-1} \text{ cm}^{-2}]$						
	UM196	Q0044-273	UM667	Q0046-282	Q0103-294	Q0103-260	4C25.05
OVI 1034	11.05±1.0	1.8±0.20	6.7±1.0	2.27±0.21	—	8.3±2.00	—
Ly α 1215	52.1±1.0	10.40±0.50	38.0±1.0	19.90±1.00	12.00±1.00	38.9±1.20	125.1±5.0
NV 1240	14.40±1.0	3.35±0.50	9.5±1.0	7.60±1.00	3.80±0.40	8.10±0.70	42.2±3.0
OI 1304	1.40±0.2	0.34±0.08	2.37±0.3	0.70±0.10	—	3.6±0.20	9.2±0.5
CII 1335	0.66±0.15	—	0.61±0.15	0.80±0.10	—	1.9±0.30	3.1±0.4
SiIV1402	4.60±0.2	1.32±0.10	5.0±0.2	2.88±0.15	1.44±0.30	6.1±0.30	10.4±1.0
CIV 1549	25.6±1.0	8.10±0.30	11.75±0.7	4.89±0.10	10.64±0.30	14.6±0.90	54.6±4.0
HeII 1640	3.2±0.3	1.74±0.40	1.31±0.2	0.73±0.15	1.13±0.20	2.94±0.30	6.9±1.0
OIII] 1663	1.76±0.2	0.31±0.06	0.66±0.2	—	0.80±0.20	1.57±0.30	2.3±0.5
NIII] 1750	0.72±0.2	—	—	—	0.38:	—	—
FeII UV191	—	—	—	—	0.21:	0.84±0.20	2.5±0.5
AlIII 1859	—	—	0.75±0.3	—	—	1.23±0.30	1.2±0.3
SiIII] 1892	—	—	—	—	—	—	1.2±0.3
CIII] 1909	7.5±0.6	0.99±0.06	5.07±0.3	1.63:	2.88±0.40	6.6±0.40	17.9±2.0
FeII UV2100	0.73±0.2	—	—	—	0.25±0.05	—	5.2±0.3
α	1.18	0.56	0.62	0.13	1.21	0.34	0.59
	Q0216+0803	HS1425+60	Q1548+0917	PC1640+4711	HS1700+64	Pks2126-15	PC2132+0126
OVI 1034	4.9±0.8	—	—	—	—	—	4.97±0.3
Ly α 1215	67.4±4.0	525±20	54.9±4.0	17.7±4.0	340±20	79±4	18.87±1.0
NV 1240	17.9±3.0	58.6±5.0	32.0±2.0	3.9±0.8	134.5±6.0	24.4±2.0	4.95±0.5
OI 1304	8.3±1.0	26.2±4.0	3.9±0.6	—	16.0±1.0	4.8±0.6	2.1±0.3
CII 1335	3.9±0.7	16.1±4.0	—	—	14.7±0.5	1.5±0.2	0.85±0.2
SiIV1402	11.3±1.0	56.3±3.0	12.2±1.0	0.9±0.3	85.7±1.0	10.6±1.0	1.96±0.2
CIV 1549	44.8±2.0	125±5.0	42.3±2.0	6.6±0.6	114.3±3.0	31.8±2.0	6.20±0.5
HeII 1640	4.75±0.7	9.3±1.0	5.8±0.7	1.4±0.4	7.9±0.5	3.7±0.3	0.67±0.1
OIII] 1663	2.4±0.5	8.7±1.0	3.0±0.7	0.4±0.2	4.3±0.4	3.1±0.3	0.53±0.1
NIII] 1750	—	—	2.2±0.5	—	4.5±0.6	—	—
FeII UV191	—	14.4±1.0	—	—	4.0±0.6	—	—
AlIII 1859	1.6±0.4	15.7±1.0	—	1.0±0.3	12.0±2.0	1.1±0.2	—
SiIII] 1892	—	—	—	—	—	—	—
CIII] 1909	7.74±0.8	76.8±3.0	9.4±1.0	2.9±0.5	81.5±6.0	23.5±2.0	2.90±0.3
FeII UV2100	—	—	—	—	12.3±1.0	—	—
α	0.33	0.89	0.36	0.54	0.66	1.09	1.45
	Q2231-0015	UM659					
OVI 1034	10.1±2.0	6.04±0.3					
Ly α 1215	112.7±5.0	34.6±1.0					
NV 1240	16.3±0.7	3.73±0.2					
OI 1304	5.87±0.5	2.67±0.3					
CII 1335	2.4±0.3	0.91±0.2					
SiIV1402	7.14±0.5	2.20±0.3					
CIV 1549	23.23±1.0	10.57±0.5					
HeII 1640	4.54±0.5	1.01±0.2					
OIII] 1663	4.3±0.5	0.91±0.2					
NIII] 1750	2.94±0.4	—					
FeII UV191	1.61±0.3	—					
AlIII 1859	1.12±0.2	0.50±0.1					
SiIII] 1892	1.42±0.3	—					
CIII] 1909	8.59±0.7	3.0±0.3					
FeII UV2100	—	—					
α	0.78	1.05					

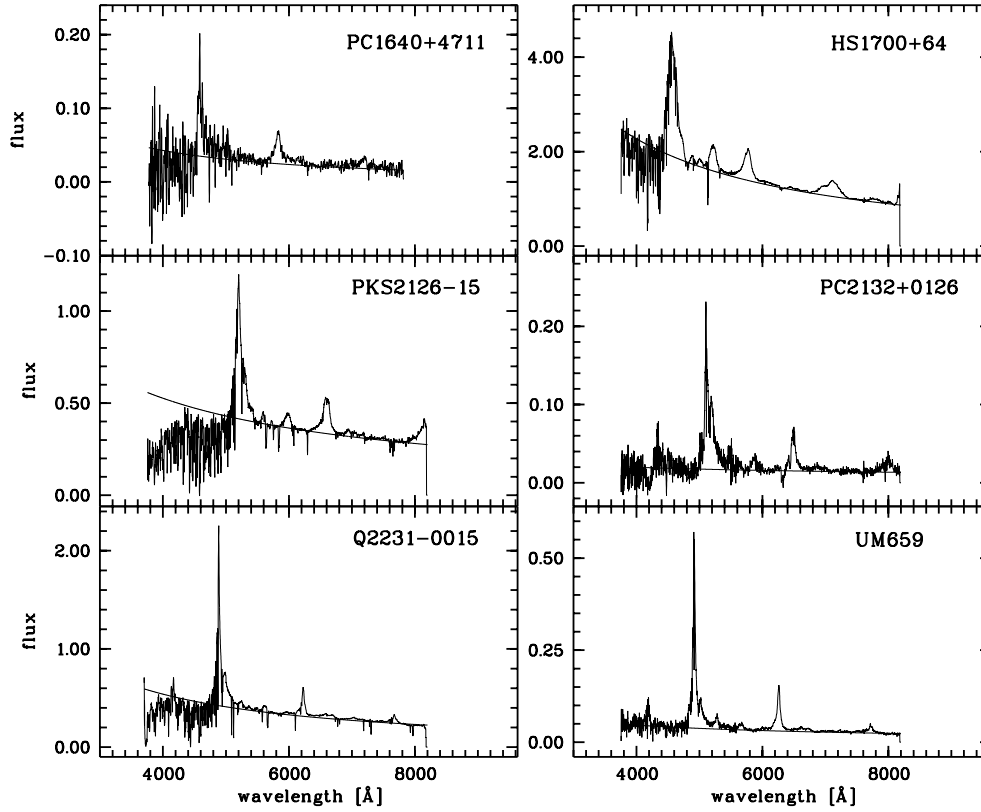


Fig. 2. The spectra of the observed QSOs. The flux is given in units of $10^{-15} \text{ erg s}^{-1} \text{ cm}^{-2} \text{ \AA}^{-1}$. For each QSO the corresponding power law fit $F_\nu \sim \nu^{-\alpha}$ of a nonstellar continuum is displayed.

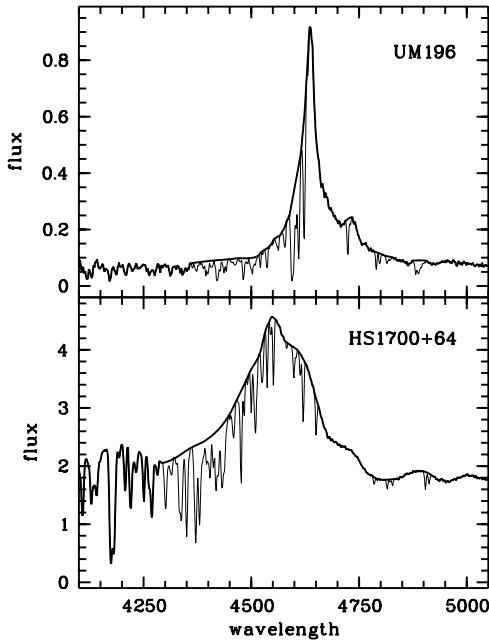


Fig. 3. Correction of absorption systems in the emission line profile of $\text{Ly}\alpha$ is displayed for the narrow-line quasar UM 196 (top panel) as well as for the broad-line quasar HS 1700+64 (bottom panel). The observed line profiles are plotted as a thin line and the corrected profiles are displayed as bold lines.

blended by other strong emission lines we used the CIV1549 emission line as a template profile. Since CIV1549, NV1240,

and HeII1640 are high ionization lines (HIL) this approach can be justified. Assuming the line profiles have the same line width and shape the CIV profile we scaled and subtracted it from the emission line profile to measure after transforming both into velocity space. For the transformation of the line profile into velocity space we used the redshifts given in Table 1. This approach does not take into account the contribution of a narrow line component and assumes implicitly that the narrow line contribution of CIV1549 is of the same order for the other broad emission lines which we fitted. Since the broad emission line profiles of the quasars which we studied show no indication of a significant narrow line component, for example in the residua after subtraction of the scaled CIV1549 profile, this influence was neglected.

In Fig. 4 and 5 typical results of the deblending of the $\text{Ly}\alpha$, NV1240 and CIV1549, HeII1640, OIII]1663 line profile complexes are shown. This method could be applied to almost all emission lines, solely the $\text{Ly}\alpha$ profile differs from the CIV1549 profile. The results of the flux measurements of our quasar sample are given in Table 2. The given uncertainties are estimated from the line fit using the scaled CIV1549 line profile to obtain a reasonable residuum. For the stronger lines like $\text{Ly}\alpha$, NV1240, SiIV1400, CIV1549, and CIII]1909 the errors are of the order of 5–10% while it is $\sim 20\%$ or even more for the weaker lines. In addition to the flux measurements a power law fit representing the non-stellar continuum was calculated. The power law $F_\nu \propto \nu^{-\alpha}$ was calculated using those spectral regions which are free of detectable emission lines to fix the continuum intensity. The spectral indices α are given in Table 2.

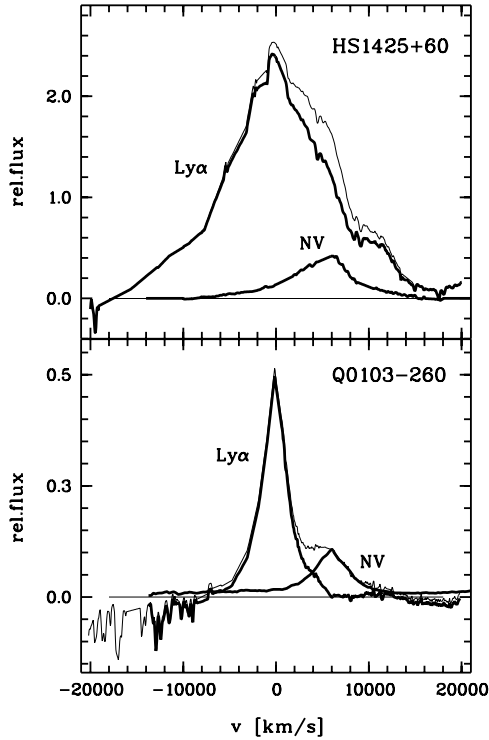


Fig. 4. Reconstruction of the $\text{Ly}\alpha$, $\text{NV}1240$ line profile complex. The individual profiles are displayed as bold lines and the observed line profile is displayed as thin line.

We calculated the diagnostic line ratios $\text{NV}1240/\text{CIV}1549$ and $\text{NV}1240/\text{HeII}1640$ using the flux measurements given in Table 2. Both line ratios (Fig. 6) are in good agreement with the results obtained by Hamann & Ferland (1992, 1993) for quasars at similar redshift. These individual line ratios were used to calculate an average line ratio yielding $\text{NV}1240/\text{CIV}1549 = (0.7 \pm 0.3)$ and $\text{NV}1240/\text{HeII}1640 = (5.9 \pm 3.6)$. The dotted lines (Fig. 6) indicate the line ratios which are expected for the conditions of the BELR gas assuming solar metallicity (Hamann & Ferland 1999). The observed line ratios are obviously larger than those for solar metallicities indicating super-solar abundances. The $\text{NV}1240/\text{HeII}1640$ line ratio we derived for the quasar spectra contribute a significant number of new measurements for the redshift range larger than $z \gtrsim 3$.

We also calculated the mean $\text{NIII}]1750/\text{OIII}]1663$ line ratio for the four quasars we could measure the $\text{NIII}]1750$ emission line flux. The average of this ratios amounts to $\text{NIII}]1750/\text{OIII}]1663 = (0.72 \pm 0.26)$. This rms-value does not take into account the uncertainties of the individual line measurements of $\text{OIII}]1663$ and $\text{NIII}]1750$.

4. Discussion

The obtained emission-line ratios of $\text{NV}1240/\text{CIV}1549$ and $\text{NV}1240/\text{HeII}1640$ were used to estimate the metallicity of the line emitting gas. The conversion of observed emission line ratios to relative abundances is affected with several severe uncer-

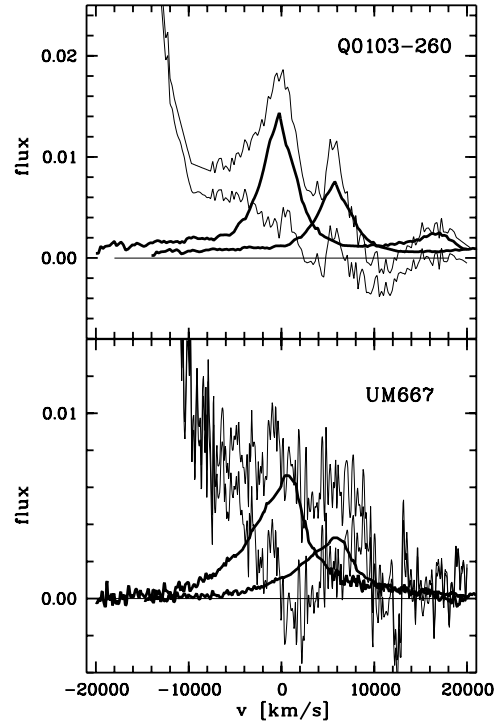


Fig. 5. Reconstruction of the $\text{CIV}1549$, $\text{HeII}1640$, $\text{OIII}]1663$ line profile complex transformed to velocity space centered to $\text{HeII}1640$. The individual profiles, as scaled template profiles, are displayed as bold lines, the observed line complex is shown as the upper thin line, and the residuum is displayed as the lower thin line. The flux is given in arbitrary units.

tainties. One has to guarantee for example that the emission lines which are studied originate in the same region of the BLR under comparable conditions of the gas. Even the input parameters of standard BLR photoionization models are uncertain within a factor of 2–3. A detailed discussion of the current limitations of the method can be found in Baldwin et al. (1996), Ferland et al. (1996), or Hamann & Ferland (1999). In spite of these uncertainties the emission line ratios of dedicated lines can be used to estimate relative abundance ratios. These results can be regarded as lower limits of the metallicity of the gas (e.g. Ferland et al. 1996).

Our estimate is based on the model calculations Hamann & Ferland (1992, 1993) presented. They computed for a large range of metallicities several evolutionary scenarios. They varied the slope of the IMF, the evolutionary time scale for the star formation, as well as the low mass cutoff of the IMF. They concluded that the high metallicities observed in high redshift quasars can be achieved only in models with rapid star formation (RSF) comparable to models of giant elliptical galaxies and a more shallow IMF than the IMF provided by studies of the solar neighborhood, i.e. more massive stars are present in RSF models.

To derive an estimate of the metallicity we compared our results with their models for two enrichment scenarios (Hamann & Ferland 1999) with a fixed density of the line emitting gas. The

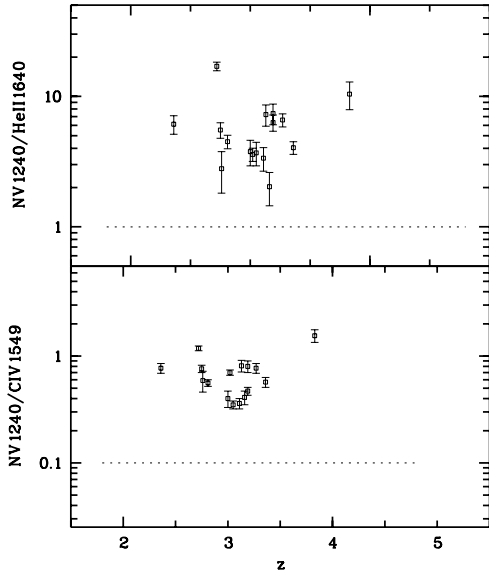


Fig. 6. NV1240/CIV1549 and NV1240/HeII1640 as a function of redshift. The dotted lines indicate the line ratios which are expected for the conditions of the BELR gas assuming solar metallicity (Hamann & Ferland 1999).

first scenario is characterized by scaled solar metallicities, i.e. with relative solar abundance ratios. The second model assumes abundance ratios which are given by the rapid star formation model. In contrast to the scaled solar metallicity model in the RSF model the abundance of nitrogen as a secondary element is built up quadratically with metallicity while primary elements like carbon or oxygen are built up only linearly.

Within the framework of the scaled solar abundance model the observed NV1240/HeII1640 ratio indicates supersolar metallicities. The derived abundance of the line emitting gas ranges from $\sim 7Z_{\odot}$ (Q0044-273) up to $\sim 43Z_{\odot}$ (HS1700+64). Computing the average of the metallicities indicated by NV/HeII yields $Z \simeq 20Z_{\odot}$. In contrast to this result the observed NV1240/CIV1549 line ratios yield even higher abundances which are of the order of $Z \simeq 100Z_{\odot}$. For several quasars we could calculate the OVI1034/HeII1640 line ratio. The corresponding abundances are in good agreement with the values obtained from NV1240/HeII1640. But the metallicity estimate based on the NIII]1750/OIII]1663 line ratio is consistent with metallicities of the order of $\sim 100Z_{\odot}$. The line ratios of NV/HeII and NV/CIV yield significantly different ranges for the metallicity of the line emitting gas assuming the scaled solar abundances model (Hamann & Ferland 1999). The line ratios combining nitrogen and carbon or oxygen indicate abundances of the order of $\sim 100Z_{\odot}$. This might be due to the strength of the nitrogen emission lines as a result of a stronger enhancement of N in comparison to C and O.

The rapid star formation (RSF) model yields higher than solar abundances for the broad emission-line gas, too. However, the range of the supersolar abundances is consistent based on the NV1240/CIV1549 and NV1240/HeII1640 line ratios. A supersolar metallicity ensues from the NV1240/CIV1549

Table 3. The derived relative abundance of the line emitting gas given in units of solar metallicity Z_{\odot} . The estimates based on the calculations made with the rapid star formation scenario (Hamann & Ferland 1999). The metallicity is given in units of solar metallicities Z_{\odot} .

object	NV/CIV	NV/HeII	OVI/HeII	NIII]/OIII]
UM196	9.6	4.0	16.6	1.8
Q0044-273	7.5	2.1	4.0	—
UM667	12.0	5.7	20.4	—
Q0046-282	17.4	7.5	15.0	—
Q0103-294	6.7	3.1	—	—
Q0103-260	9.8	3.6	14.7	—
4C25.05	11.7	5.1	—	—
Q0216+0803	7.4	3.4	4.0	—
HS1425+60	8.4	5.1	—	—
Q1548+0917	11.4	4.8	—	2.9
PC1640+4711	10.2	2.7	—	—
HS1700+64	15.1	10.1	—	4.2
PKS2126-15	11.7	5.3	—	—
PC2132+0126	11.9	6.1	25.5	—
Q2231-0015	11.5	3.3	12.5	2.8
UM659	6.6	3.4	22.3	—

line ratio which ranges from $\sim 7Z_{\odot}$ up to $\sim 17Z_{\odot}$ with an average of $Z \simeq 11Z_{\odot}$. The NV1240/HeII1640 line ratio yields an average overabundance of the studied emission line gas of $Z \simeq 5Z_{\odot}$ ranging from $\sim 2Z_{\odot}$ up to $10Z_{\odot}$ for the individual quasars (Table 3). Both line ratios indicate an average enhancement of the metallicity of the line emitting gas for the studied quasars ($2.4 \leq z \leq 3.8$) of the order of $Z \simeq 8Z_{\odot}$. This result is supported by the line ratios of OVI1034/HeII1640 and NIII]1750/OIII]1663 which could be measured for a few quasars we observed. The OVI1034/HeII1640 line ratio also indicates a higher than solar abundances. However, the scatter of the derived metallicities is large due to the obvious difficulty in measuring the line flux of OVI1034 and HeII1640. The obtained estimate of the metallicity based on the OVI/HeII line ratio covers a range of $\sim 4Z_{\odot} - \sim 25Z_{\odot}$. This result is in good agreement with the high abundances provided by the NV/CIV and NV/HeII line ratios.

In four of the observed quasars, UM196, Q1548+0917, HS1700+64, and Q2231-0015, we could also detect the important intercombination line NIII]1750. This line was used together with OIII]1663 and CIII]1909. The line ratios NIII]/OIII] and NIII]/CIII] indicate only moderate oversolar abundances but again the metallicity of the gas is in the range of $Z \simeq 3Z_{\odot}$.

In contrast to the scaled solar abundance model the RSF scenario provide consistent ranges for the metallicity of the line emitting gas based on different line ratios. Especially the line ratios of nitrogen as a secondary element with carbon or oxygen as primary elements provide evidence for an enrichment of nitrogen $\sim Z^2$ while the portion of carbon and oxygen is enhanced $\sim Z$ as predicted by the RSF model (cf. Ferland & Hamann 1992, 1993).

The derived supersolar abundances of the line emitting broad-line region gas can be used to date the age of the first

star formation epoch. We estimated the redshift z_f for several settings of Ω_M , Ω_Λ , and H_0 . The evolutionary time scale was set to 0.5, 1.0, and 2.0 Gyr. With the diagrams given in Carroll et al. (1992), Perlmutter et al. (1999), Yoshii et al. (1998), and Hamann & Ferland (1999) we derived z_f for our quasar sample. For a universe with $\Omega_M=1$ (Einstein, de Sitter) the evolutionary time scale has to be of the order of less than or approximately ~ 0.5 Gyr. For longer time scales the redshift of the first star forming epoch is larger than $z \sim 10$. Furthermore, for $z \geq 4$ the age of the universe starts to become less than the evolutionary time scale. Generally, the Einstein, de Sitter case requires $z \geq 10$ and $H_0 \leq 40 \text{ km s}^{-1} \text{ Mpc}^{-1}$. However, current measurements of H_0 and Ω_M are in serious conflict with this.

More reasonable estimates are provided by models characterized by $\Omega_M=0.3$ (open universe), $\Omega_M=0.3$, $\Omega_\Lambda=0.7$ (flat, Λ dominated universe, cf. Carlberg et al. 1999; Perlmutter et al. 1999), and $H_0=65 \text{ km s}^{-1} \text{ Mpc}^{-1}$. Assuming an evolutionary time scale of $\tau_{evol} = 0.5$ Gyr the epoch of the first star formation can be dated to $z_f \simeq 4.5$ for quasars with $3 \lesssim z \lesssim 4$ and supersolar abundances. For longer evolutionary time scales of $\tau_{evol} = 1$ Gyr the first violent star formation should took place at $z_f \simeq 6$ to 10 and at least $z_f \gtrsim 10$ for $\tau_{evol} = 2$ Gyr. For redshifts of $z \simeq 4$ or even larger already an evolutionary time scale of ~ 1 Gyr indicates $z_f \gtrsim 10$. If $\tau_{evol} \simeq 2$ Gyr the detection of supersolar metallicity for quasars with $z \simeq 4$ to 5 requires $\Omega_M \leq 0.3$. Otherwise the universe would not be old enough for the assumed time scale to produce the observed metal enrichment of the gas. This might be taken as some evidence for short evolutionary time scales for the first violent star formation epoch. The quasar with the currently highest known redshift of $z = 5.0$ (SDSSp J033829.31+002156.3, Fan et al. 1999) provides some hint for a metal abundances comparable to the quasars observed at redshift $z \simeq 4$ (Dietrich et al. 1999). Hence, the evolutionary time scale for this object should be less than ~ 1 Gyr and the studied quasars favor models with $\Omega_M \leq 0.3$, $\Omega_\Lambda \simeq 0.7$, and $H_0=65 \text{ km s}^{-1} \text{ Mpc}^{-1}$.

5. Conclusion

We observed a sample of 16 high redshift quasars with $2.4 \lesssim z \lesssim 3.8$ with moderate spectral resolution. We used the emission-line fluxes of NV1240, CIV1549, and HeII1640 to estimate the metallicity of the line emitting gas. We analysed the derived line ratios within the frame work of models presented by Hamann & Ferland (1992, 1993, 1999). The scaled solar abundance model yields inconsistent values for the metallicity provided by NV1240/CIV1549 and NV1240/HeII1640 line ratios. The rapid star formation scenario is successful in indicating the same range of overabundance on base of those line ratios. We estimated an abundance of $Z \simeq 8 Z_\odot$ given by NV/CIV and NV/HeII. For several quasars of our sample we could also use OVI1034 and the intercombination lines OIII]1663, NV]1750, and CIII]1909 to obtain the relative abundances. These line ratios indicate although with larger scatter within the rapid star formation model metallicities of the order of $Z \simeq (3 - 20) Z_\odot$.

With an evolution time scale of approximately 1 Gyr the beginning of the first violent star formation could be determined to a redshift of $z_f \simeq 6$ to 10. This result is consistent with cosmological models with $\Omega_M \simeq 0.3$, $\Omega_\Lambda \simeq 0.7$, and $H_0 \simeq 65 \text{ km s}^{-1} \text{ Mpc}^{-1}$. In contrast models with significantly smaller H_0 and higher Ω_M require a much shorter evolutionary time scale otherwise the universe will not be old enough at redshift of $z \simeq 4$.

Acknowledgements. We thank Hans Hagen for kindly providing the coordinates of two quasars of the Hamburg QSO survey for this investigation. We would like to express sincere thanks to the staff of the Paranal observatory for the efficient and friendly support of the FORS commissioning team and the commissioning team itself. We would also like to thank Fred Hamann for many suggestions and discussions improving the paper. The investigators have benefited from support from: SFB 328 D and SFB 439 (Landessternwarte Heidelberg) DFG grant Ko 857/13-1 (Universitätssternwarte Göttingen).

References

- Baldwin J.A., Netzer H., 1978, ApJ 226, 1
 Baldwin J.A., Ferland G.F., Korista K.T., Verner D., 1995, ApJ 455, L119
 Baldwin J.A., Ferland G.F., Korista K.T., et al., 1996, ApJ 461, 664
 Burstein D., Heiles C., 1982, AJ 87, 1165
 Carlberg R.G., Yee H.K.C., Morris S.L., et al., 1999, ApJ 516, 552
 Carroll S.M., Press W.H., Turner E.L., 1992, Ann. Rev. Astron. Astrophys. 30, 499
 Condon J.J., Hicks P.D., Jauncey D.L., 1977, AJ 82, 692
 Davidson K., 1977, ApJ 218, 20
 Dietrich M., Appenzeller I., Wagner S.J., et al., 1999, A&A, in press
 Fan X., Strauss M.A., Schneider D.P., et al., 1999, AJ 118, 1
 Ferland G.F., Peterson B.M., Horne K., Welsh W.F., Nahar S.N., 1992, ApJ 387, 95
 Ferland G.F., Baldwin J.A., Korista K.T., et al., 1996, ApJ 461, 683
 Filippenko A.V., 1982, PASP 94, 715
 Foltz C.B., Chaffee F.H., Hewett P.C., et al., 1989, AJ 98, 1959
 Gaskell C.M., Shields G.A., Wampler E.J., 1981, ApJ 249, 443
 Hagen H., 1993, private communication
 Hamann F., Ferland G.F., 1992, ApJ 381, L53
 Hamann F., Ferland G.F., 1993, ApJ 418, 11
 Hamann F., Ferland G.F., 1999, Ann. Rev. Astron. Astrophys. 37, 487
 Hewett A., Burbidge G., 1993, ApJS 87, 451
 Horne K., 1986, PASP 98, 609
 Korista K.T., Hamann F., Ferguson J., Ferland G.J., 1996, ApJ 461, 641
 Korista K.T., Baldwin J.A., Ferland G.J., Verner D., 1997, ApJS 108, 401
 MacAlpine G.M., Smith S.B., Lewis D.W., 1977, ApJS 35, 197
 MacAlpine G.M., Feldman F.R., 1982, ApJ 261, 412
 Massey P., Strobel K., Barnes J.V., Anderson E., 1988, ApJ 328, 315
 Oke J.B., 1990, AJ 99, 1621
 Oke J.B., Gunn J.E., 1983, ApJ 266, 713
 Olsen E.T., 1970, AJ 75, 764
 Osmer P.S., 1980, ApJ 237, 666
 Osmer P.S., Porter A.C., Green R.F., 1994, ApJ 436, 678
 Perlmutter S., Aldering G., Goldhaber G., et al., 1999, ApJ 517, 565
 Peterson B.M., 1993, PASP 105, 1084
 Pettini M., 1999, in Proc. of ESO Workshop ‘Chemical Evolution from Zero to High Redshift’, ed. J. Walsh & M. Rosa, LNP, in press

- Rees M., Netzer H., Ferland G.J., 1989, ApJ 347, 640
Reimers D., Clavel J., Groote D., 1989, A&A 218, 71
Sargent W.L.W., Steidel C.C., Boksenberg A., 1989, ApJS 69, 703
Savage B.D., Mathis J.S., 1979, Ann. Rev. Astron. Astrophys. , 17, 73
Schmidt M., Schneider D.P., Gunn J.E., 1987, ApJ 316, L1
Schneider D.P., Schmidt M., Gunn J.E., 1991, AJ 101, 2004
Schneider D.P., Bahcall J.N., Saxe D.H., et al., 1992, PASP 104, 678
Schwarz H.E., Melnick J., 1993, The ESO Users Manual, p. 24
Shields G.A., 1976, ApJ 204, 330
Steidel C.C., Sargent W.L.W, Dickinson M., 1991, AJ 101, 1187
Turnshek D.A., 1990, AJ 99, 1243
Uomoto A. 1984, ApJ 284, 497
Wheeler J.C., Sneden C., Truran J.W., 1989, Ann. Rev. Astron. Astrophys. 27, 279
Wolfe A.M., Turnshek D.A., Smith H.E., Cohen R.D., 1986, ApJS 61, 249
Yoshii Y., Tsujimoto T., Kawara K., 1998, ApJ 507, L113